Resonant inelastic x-ray scattering at the Fe L_3 edge of the one-dimensional chalcogenide $BaFe_2Se_3$

C. Monney,[1,2] A. Uldry,[3] K. J. Zhou,[1,4] A. Krzton-Maziopa,[5,6] E. Pomjakushina,[5] V. N. Strocov,[1] B. Delley,[3] and T. Schmitt[1,*]

[1]*Research Department Synchrotron Radiation and Nanotechnology, Paul Scherrer Institut, CH-5232 Villigen PSI, Switzerland*

[2]*Fritz-Haber-Institut der Max Planck Gesellschaft, Faradayweg 4-6, D-14195 Berlin, Germany*

[3]*Condensed Matter Theory Group, Paul Scherrer Institut, CH-5232 Villigen PSI, Switzerland*

[4]*Diamond Light Source, Harwell Science and Innovation Campus, Didcot, Oxfordshire, OX11 0DE, United Kingdom*

[5]*Laboratory for Development and Methods, Paul Scherrer Institut, CH-5232 Villigen PSI, Switzerland*

[6]*Faculty of Chemistry, Warsaw University of Technology, Noakowskiego 3, PL-00664 Warsaw, Poland*

(Received 21 December 2012; revised manuscript received 24 June 2013; published 3 October 2013)

We present an electronic structure study of the quasi-one-dimensional chalcogenide $BaFe_2Se_3$ using resonant inelastic x-ray scattering (RIXS) at the Fe L_3 edge. In addition to broad spectral contributions from fluorescence, sharp peaks are seen at the low-energy end of the spectra, suggesting the coexistence of both band and localized properties in this compound up to the antiferromagnetic transition temperature. The width of the fluorescence line can be accounted for by band structure calculations, while the positions of the sharp peaks are in good agreement with crystal-field multiplet calculations. At measurement temperatures below 300 K, the temperature dependence of the low-energy part of the spectra is accounted for by the changes in thermal occupation of closely lying energy states. At 300 K, however, a substantial broadening of the spectra is observed at low-energy loss, which is consistent with the closure of the antiferromagnetic band gap.

DOI: 10.1103/PhysRevB.88.165103 PACS number(s): 78.70.En, 71.70.Ch

I. INTRODUCTION

In recent years, iron-based pnictides and chalcogenides[1–3] have attracted a tremendous interest in the framework of high-temperature superconductivity (HTSC). As for the cuprate materials,[4–6] the origin of superconductivity in these new families is still very controversial. While the similarity of their respective phase diagrams upon electron and hole doping calls for a common mechanism leading to superconductivity, important differences raise doubts on such a mechanism. In particular, the nature of magnetism in pnictides and chalcogenides, namely itinerant versus localized magnetic moments,[7–9] as well as the strength of electronic correlations are disputed.

The two-dimensional nature of HTSC triggered a lot of interest in structurally simpler model materials of low dimensionality, like cuprate chains and ladder compounds.[10,11] The only close relative of the iron-based superconductors of low dimension discovered so far is the ladder system $BaFe_2Se_3$ and, surprisingly, has been poorly studied. $BaFe_2Se_3$ consists of Fe_2Se_3 ladders doped by Ba ions (see Fig. 1), where Fe is in approximately tetrahedral coordination with Se, building up an elementary basis common to all pnictides and chalcogenides. Nominally, an oxidation state Fe^{2+} is expected for the Fe ions, leading to a d^6 electronic configuration of the valence shell. $BaFe_2Se_3$ has been recently shown to undergo a second-order phase transition towards a block antiferromagnetic (AFM) ground state at $T_{AFM} = 250$ K, with Fe magnetic moments (perpendicular to the Fe ladder) reaching the value of $2.1\mu_B$ at the lowest temperature.[12,13] So far, no experimental study of its electronic structure has been done and only first-principles calculations have been carried out.[14] The results of resistivity measurements[15] suggested that $BaFe_2Se_3$ is a semiconductor with an activation energy of 0.18 eV.

In this work, we investigate the electronic structure of $BaFe_2Se_3$ by means of resonant inelastic x-ray scattering at the Fe L_3 edge. RIXS has recently proven to be very powerful to probe low dimensional systems.[16,17] Our study suggests that this low-dimensional chalcogenide exhibits a mixed character between a band and a correlated material: in addition to a broad spectral response from fluorescence, sharp low-energy excitations can be identified. The present work finds correlated electron multiplet resonances in $BaFe_2Se_3$, which was previously regarded as a weakly correlated electron system.

A substantial broadening of this part of the spectra is observed as the system leaves the block antiferromagnetic phase. At lower temperatures, however, the small temperature dependence is explained by changes in thermal occupation of close-lying energy levels in the RIXS initial states.

The experimental RIXS measurements are described in Sec. II and discussed in Sec. III. Section IV presents the band structure of $BaFe_2Se_3$ calculated with the DMol^3 code and multiplet calculations for $BaFe_2Se_3$ with the crystal-field MULTIX code.[18] Some aspects of the multiplet calculations are discussed in detail in Sec. V, in particular, the nature of the multiplet state and the temperature dependence at low temperature. Conclusions are given in Sec. VI.

II. EXPERIMENTAL

RIXS experiments were performed at the ADRESS beamline[19] of the Swiss Light Source, Paul Scherrer Institut, using the SAXES spectrometer.[20] A scattering angle of 130° was used and the sample was measured at the specular position, i.e., at an incidence angle of 65° (see, e.g., Fig. 1 in Ref. 16 for a sketch of the scattering geometry), meaning that no light momentum is transferred to the system along the chain direction. The combined energy resolution was 120 meV at the Fe L_3 edge (with an incident photon energy $\hbar\omega_i \sim 710$ eV). $BaFe_2Se_3$ single crystals[12] were cleaved *in situ* at the pressure of about 5×10^{-10} mbar and at 15 K, resulting in surfaces oriented perpendicular to the [100] axis. As reported in Ref. 12, the $BaFe_2Se_3$ crystals consist of numerous blocks misaligned

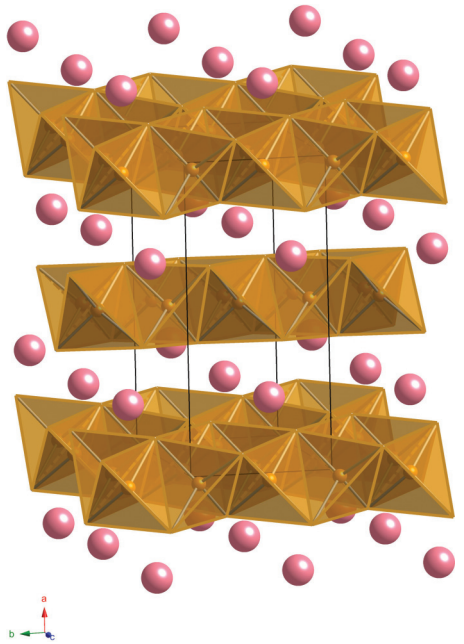

FIG. 1. (Color online) Crystal structure of $BaFe_2Se_3$. The coordination of the Fe atoms with Se atoms situated at the corners of the polyhedra is emphasized, with Ba (pink spheres) atoms in between. The double chains of FeSe tetrahedra are edge shared and propagate along the *b* axis.

by a rotation, presumably along the longest *a* axis. As a consequence of this mosaicity, only limited information can be gained from a RIXS polarization study. Therefore we focus in this article on the energy and temperature dependence of the spectra. All the RIXS spectra were normalized to the acquisition time.

III. Fe L_3 EDGE DATA

The x-ray absorption spectroscopy (XAS) spectrum of $BaFe_2Se_3$ has been measured at 15 K in total fluorescence yield mode at the Fe *L* edge. Figure 2(b) shows the L_3-edge results and Fig. 6(b) (solid blue line) the whole L_3-L_2 range. No sharp absorption peaks are observed in this spectrum, that exhibits a similar spectral shape as Fe-pnictide materials.[21]

RIXS spectra have been acquired for incident energies $\hbar\omega_i$ across the Fe L_3-edge XAS spectrum. The data are shown in Fig. 2(a), on an energy loss scale $\hbar\Omega = \hbar\omega_f - \hbar\omega_i$, $\hbar\omega_f$ being the energy of the outgoing photons. In addition to the elastic line at zero energy loss, strong fluorescence disperses from 1 eV energy loss to higher energy losses, originating most probably from Fe 3*d* states hybridized with Se 4*p* states.[14] The fluorescence contributions shift to higher energy losses for increasing incident energies, as fluorescence in RIXS typically occurs at fixed x-ray emission energy.[22,23] Strong fluorescence contributions down to small energy losses are expected for $BaFe_2Se_3$, since this system has been identified as a semiconductor below 300 K with an activation energy of only about 0.18 eV in Ref. 15. However, a closer look at the RIXS spectra of Fig. 2(a) reveals two Raman-like peaks at 0.65 and 1.5 eV, not moving in energy position with variation of incident photon energy, superimposed on top of the fluorescence. They

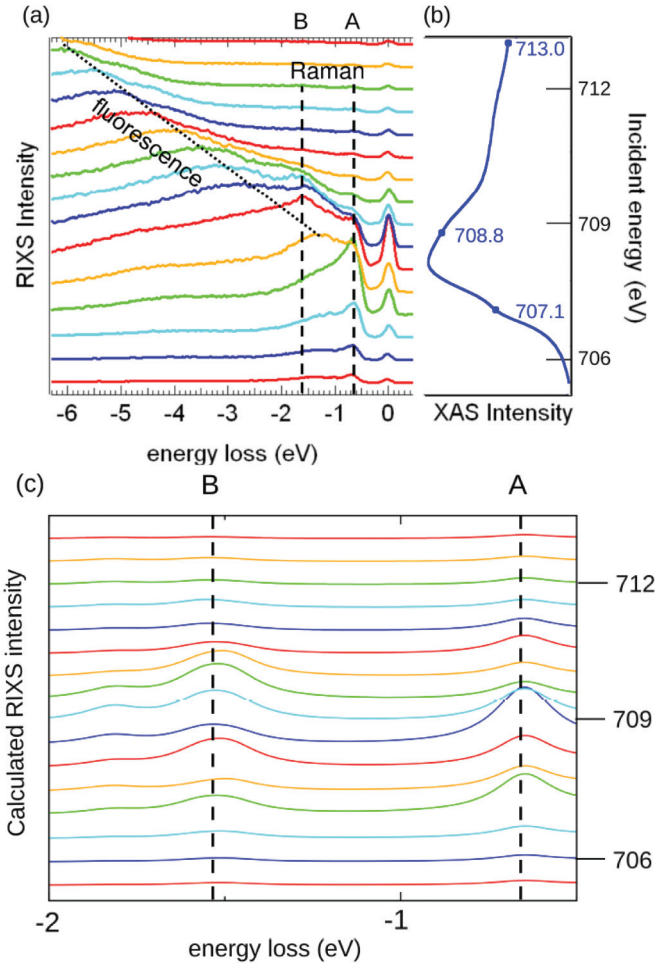

FIG. 2. (Color online) (a) RIXS spectra measured (at 15 K) for incident energies across the Fe L_3 edge (for every 0.5 eV), as indicated on the XAS spectrum on the right panel. (b) XAS spectrum at the Fe L_3 edge of $BaFe_2Se_3$, measured at 15 K in total fluorescence yield mode. (c) Calculated RIXS spectra, as explained in Sec. IV B.

are typical for crystal field excitations in correlated materials containing 3*d* transition metal elements[22,24] and are here denoted[25] as *dd* excitations. Such sharp crystal field excitation peaks have only been observed in a RIXS Fe *K*-edge study on $PrFeAsO_{1-y}$ so far, to the best of our knowledge.[26] In the $PrFeAsO_{1-y}$ RIXS study, a relatively weak fluorescence background allowed to observe *dd* excitations and charge transfer excitations, the energy that was used subsequently to infer values for intraorbital Coulomb repulsion and Hund's coupling. Furthermore, the *dd* excitations in $BaFe_2Se_3$ are similar to those observed in hematite Fe_2O_3, a correlated transition metal oxide,[21] although appearing here at smaller energy losses. Both peaks have different resonating behavior as a function of incident photon energy, the 0.65 eV Raman peak resonates on the Fe pre-L_3 edge, while the 1.5 eV Raman peak resonates just after the edge [see Fig. 2(a)].

RIXS spectra at the specific energies $\hbar\omega_i$ indicated by full circles on the XAS spectrum in Fig. 2(b) (measured at 15 K) are shown in Fig. 3. At $\hbar\omega_i = 707.1$ eV (Fe pre-L_3 edge), the RIXS spectrum (in red, continuous line) exhibits a sharp Raman peak at 0.65 eV energy loss, riding on top of the

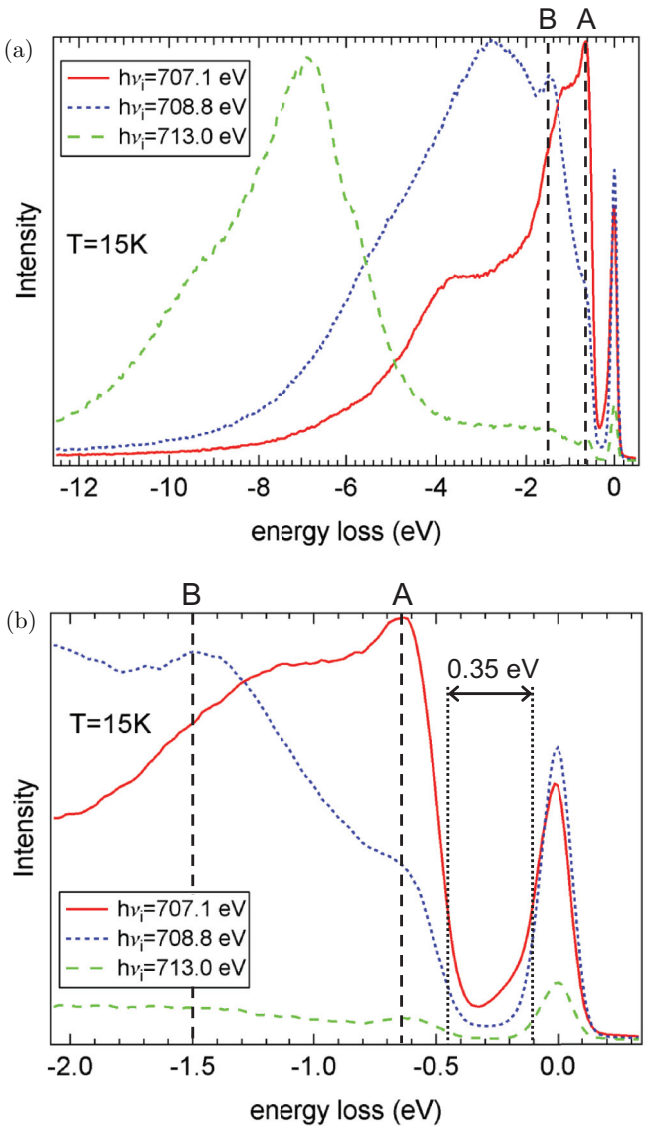

FIG. 3. (Color online) (a) RIXS spectra measured for selected incident energies at the Fe L_3 edge (at 15 K). (b) The same spectra, zoomed into the low-energy-loss region.

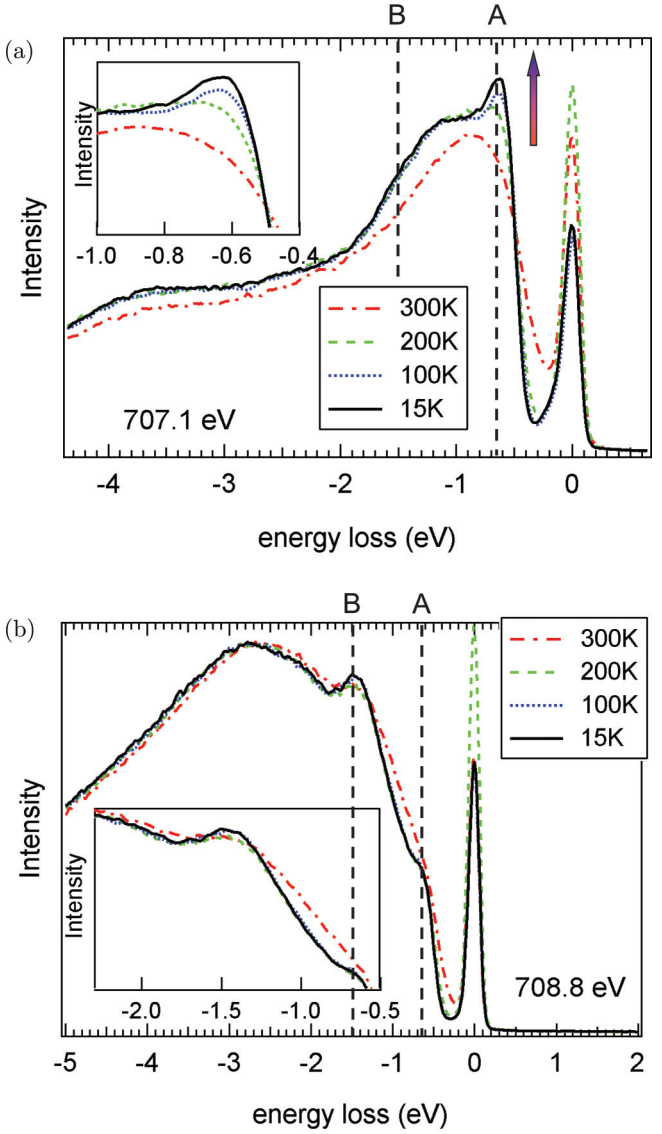

FIG. 4. (Color online) Temperature dependent RIXS spectra measured with (a) $\hbar\omega_i = 707.1$ and (b) 708.8 eV, respectively. The spectra have been normalized with respect to the acquisition time.

broad fluorescence signal. At $\hbar\omega_i = 708.8$ eV (just after the Fe L_3-edge) (blue dotted line), the fluorescence gets stronger, but shifts to higher energy losses, revealing thereby another Raman peak at 1.5 eV energy loss. At the same time, the 0.65 eV Raman peak is only visible as a shoulder. As the incident energy is detuned away from the resonance (green dashed line), at $\hbar\omega_i = 713.0$ eV, the fluorescence gives then way to a significant long tail, which we interpret as a continuum of electron-hole pair excitations created across the gap.[27]

In Fig. 3(b), the RIXS spectra are zoomed into the low-energy-loss region in order to make better visible the Raman peaks described above. In particular, one can even observe the first Raman peak (at 0.65 eV) in the RIXS spectrum taken at $\hbar\omega_i = 713.0$ eV. Interestingly, in every RIXS spectrum, there is a small gap of approximately 0.35 eV in the excitation spectrum. Considering the semiconducting nature of this material, one could relate this value to the size of its gap. This interpretation is confirmed by the thermal activation energy fitted from resistivity data,[15] 0.18 eV, which is about half of the energy gap.[28] Saparov *et al.* infer also a gap of about 0.24 to 0.30 eV from their resistivity data, depending on the temperature range;[29] these values are smaller than the experimental estimate [see Fig 3(b)] and the calculated value (see Sec. IV A) of the present study.

Furthermore, we have measured RIXS spectra as a function of temperature. As mentioned in Introduction, $BaFe_2Se_3$ undergoes a phase transition at $T_{AFM} = 250$ K to a block AFM state below this temperature. Figures 4(a) and 4(b) shows RIXS spectra for 15, 100, 200, and 300 K, at the incident energies, $\hbar\omega_i = 707.1$ and 708.8 eV, respectively. While the fluorescence signal does not change dramatically as a function of temperature, the spectra taken at $T < T_{AFM}$ show subtle differences in the low-energy-loss part of the spectra, depending on the incident energy. A small but clear temperature dependence is seen at $\hbar\omega_i = 707.1$ eV [see Fig. 4(a)], with the peak at 0.65 eV increasing in

intensity for decreasing temperatures. At $\hbar\omega_i = 708.8$ eV [see Fig. 4(b)], the situation is less obvious, due the large fluorescence developing at resonance, thereby masking the Raman peaks. From the zoom on the 1.5 eV Raman peak in the inset, hardly any temperature effect is observed. We anticipate that differentiated temperature effects are due to the thermal occupation of excited states above the ground state. Although the effects are partially masked as a consequence of the mosaicity and band effects, such occupations open new channels for RIXS excitations;[30] this will be discussed further below.

The spectra measured at 300 K, in the nonmagnetic state above T_{AFM}, are quite peculiar in comparison to the low-temperature ones. In particular, they exhibit an increased spectral weight in the gap region between the elastic line and the first *dd* excitation. This sudden change is consistent with the collapse of the antiferromagnetic band gap at the Néel temperature in the band structure theory.

IV. THEORETICAL CONSIDERATIONS

The presence of a broad fluorescence line together with sharp low-energy excitations suggests that a full theoretical treatment should cover all regimes between weakly correlated bands to the large Hubbard U limit. No practical approach is at present able to reproduce spectra capturing multiplet features together with band aspects. In this paper, the band model of the compound is addressed by density functional theory, while the localized multiplet resonances are well captured by the crystal-field model.

A. Band structure calculations

Band structure calculations were performed with the DMol^3 code,[31,32] in the spin-unrestricted formalism. A 48-atom supercell was studied using the PBEsol[33] functional, both in the paramagnetic and in a block antiferromagnetic arrangement. For the latter, the spin configuration labeled τ_1 and pictured in Fig. 4(a) of Ref. 12 was picked. Brillouin zone integrations were done using a $8 \times 8 \times 8$ mesh and a thermal scheme with electron temperature of 0.003 Hartree. The standard DMol^3 numerical basis sets *dnd* were used. The resulting partial density of states (DoS) of Fe, as well as the band structure and total DoS are plotted in Fig. 5, for the case of the block antiferromagnet. Less than 1% of the partial DoS of Fe has a non-*d* character, so that Fig. 5(a) is also a representation of the *d* band. A gap of about 0.35 eV separates the occupied bands from the unoccupied ones. This value is remarkably close to that determined from the present RIXS measurement, as stated in Sec. III, and a little smaller than that calculated by Saparov *et al.*[29] The position of the first sharp peak in Fig. 2 indicates that a low crystal field excitation appears at 0.65 eV, as supported by multiplet calculations described further below (see Sec. V B). Hybridization broadens levels into bands. A band gap of 0.35 eV suggests that the bandwidth broadening of the ground state and the 0.65 eV levels is only of 0.3 eV each. This is also the bandwidth evaluated from the subband dispersion in Fig. 5(b). The observed width of the A peak [see Fig. 4(a)], at an estimated 0.2 eV, looks even narrower than the band theory prediction. As can be seen in Fig. 5(a), the occupied Fe band has a width of a little less than 6 eV. The unoccupied band is dominated by the *d* band minority spin, and has a width of about 1 eV.

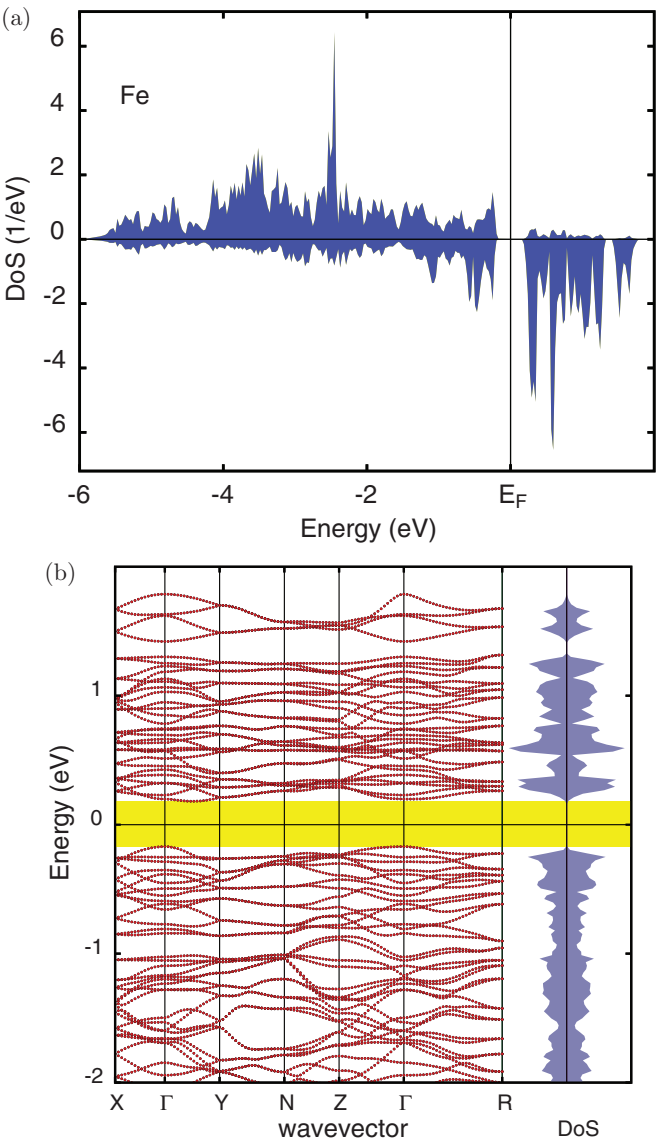

FIG. 5. (Color online) Density functional theory calculations for the block antiferromagnet $BaFe_2Se_3$. (a) Majority (upper part) and minority (lower part) partial density of states for Fe. (b) Band structure and total density of states.

Neglecting electron-electron interactions, in the spirit of the weak coupling band model, and ignoring detailed matrix element effects, the RIXS spectrum can be seen as a convolution of the occupied *d* band with the unoccupied *d* band.[22] This results in a roughly 7-eV-wide, rather featureless, spectrum with fluorescence character. This is in good agreement with the overall appearance of the experimental RIXS fluorescence spectrum.

B. Multiplet calculations

Multiplet calculations were performed with the MULTIX[18] code, which allows the specification of the crystal field *via* the charges and positions of the neighboring atoms. The valence

state of Fe in this compound is believed to be close[15] to Fe^{2+}. The ground-state configuration was therefore taken as $2p^63d^6$. XAS spectra were obtained by calculating dipolar transitions $2p^63d^6 \rightarrow 2p^53d^7$. RIXS spectra were computed from the resonant term of the Kramers-Heisenberg formula[34] with the dipolar process $2p^63d^6 \rightarrow 2p^53d^7 \rightarrow (2p^63d^6)^\star$. In this section, the assumptions and input for the calculation are discussed, as well as the scaling parameters produced by the fit to the experiments. The method applied for the inclusion of temperature effects is briefly presented, and finally the geometrical setup used for comparison with experiments is described.

1. Calculation input and parameters

As pointed out by Saparov *et al.*,[29] inconsistent unit cell dimensions have been reported for $BaFe_2Se_3$ among authors, with discrepancies put down to variations in the iron content. The crystal structure used for the multiplet calculations is that measured by neutron powder diffraction,[12] at a temperature of 2K. The reported crystallographic symmetry is *Pnma*. The Fe atom is in the local C_1 symmetry; it has four Se atoms as nearest neighbors, all at different distances, and three further Fe neighbors. With the Fe atoms forming a two-legged ladder, the bond to one of the neighbors is along a rung of the ladder and the other two along one leg. The two bonds along the leg are not of equal length, with the sequence short/long bond staggered between the two legs of the ladder. Caron *et al.*[13] showed that the displacements of the Fe atoms causing the short and long bond occur increasing with lowering of temperature. The concomitance of the displacements with the development of the long-range magnetic order led the authors to suggest significant magnetoelastic coupling in this compound.

While standard oxidation states (Ba^{2+}, Fe^{+2}, Se^{-2}) are a good starting point for allocating the point charges for the crystal field model, they often do not account for a realistic picture of charge distribution in solids. In the $BaFe_2Se_3$ case, the semiempirical charges of 2e, 1.25e, and −1.5e were allocated to Ba, Fe, and Se, respectively. This input, together with the positions of the Fe neighbors, is in principle enough to determine the energy levels of the Fe atom and to build the XAS and RIXS spectra for given polarization directions.[18] As the radial wave functions involved in the calculations are determined for a neutral atom, it is often necessary to rescale accordingly the various interactions in order to reflect the changes made on the wave functions by the bonding environment. To this purpose, semiempirical scaling parameters for the Coulomb interaction, the spin-orbit coupling and the crystal field interactions were introduced in the MULTIX[18] code, thereby accounting for screening and hybridization effects.

In the present case, a scaling parameter for the spin-orbit coupling of 0.95 and of 0.7 for the Coulomb interaction between core and valence electrons were determined by fitting the calculated XAS spectrum to the experiment [see Fig. 6(b), solid blue line]. Contrary to the XAS spectrum, the RIXS spectra are very sensitive to the crystal field. The charges and a crystal field scaling parameter of 2.97 were obtained from a fit to the *dd*-excitation part of the RIXS experiments. In order

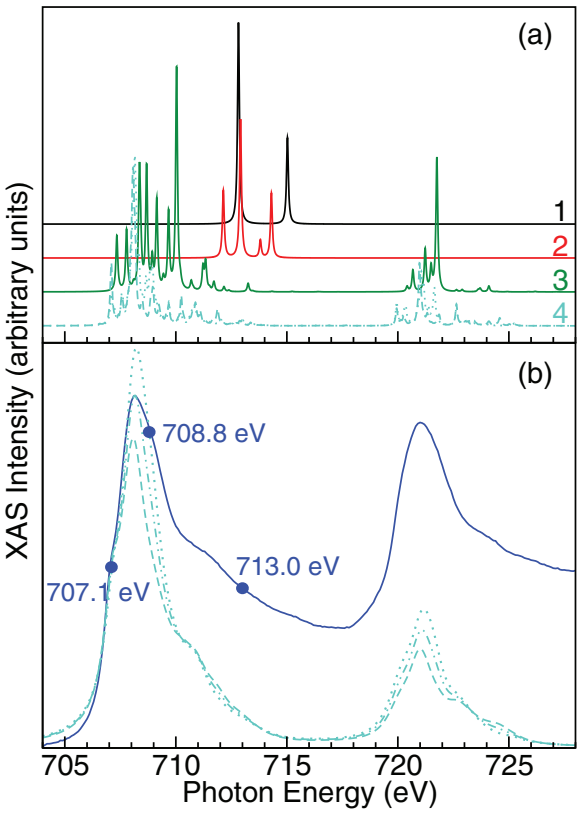

FIG. 6. (Color online) Calculated contributions to the XAS spectrum. (a) 0-K calculated contributions at constant core-hole width of 0.005 eV for Coulomb interactions between valence electrons only (1, black), for total Coulomb interaction (2, red), for Coulomb and spin-orbit interaction (3, green), and for Coulomb, spin-orbit and crystal field (4, turquoise). Dotted and dashed lines correspond to set up 1 and 2, respectively. (b) Dotted and dashed lines as in (a) but with the core-hole broadening varied linearly between 0.4 and 0.6 eV, for $T = 15$ K; dash-dot-dot line is the average between the two set ups; continuous line is the measured XAS spectrum at 15 K.

to translate the present parameters into a characteristic crystal-field splitting, the calculations were repeated for one single *d* electron with the parameters cited above, in the nonrelativistic limit. The energy difference between the barycenter of the two lowest levels and that of the three highest levels gives 1.3 eV, which can be taken as an estimate of the characteristic crystal-field splitting. As discussed in Ref. 18, reducing the Coulomb interaction and enhancing the crystal field are consistent with radial wave functions extending to adjust to a strong bonding environment. The resulting levels for the initial state of $2p^63d^6$ with Coulomb, spin-orbit and crystal-field interactions, rescaled as described above, are shown in the middle column of Fig. 7 and in the inset. This figure will be discussed further in the next section.

The simulation of core-hole spectra requires, furthermore, some assumptions about the core-hole lifetime and in the case of RIXS, the final state broadening. For the XAS spectra, the core-hole linewidth was taken to be 0.4 eV and increased linearly to 0.6 eV after the L_3 pre-edge, at around 707.4 eV. These values are slightly larger than those corresponding to the intrinsic core-hole lifetimes of transition metals[35] and account to some extent for extrinsic contributions. For RIXS,

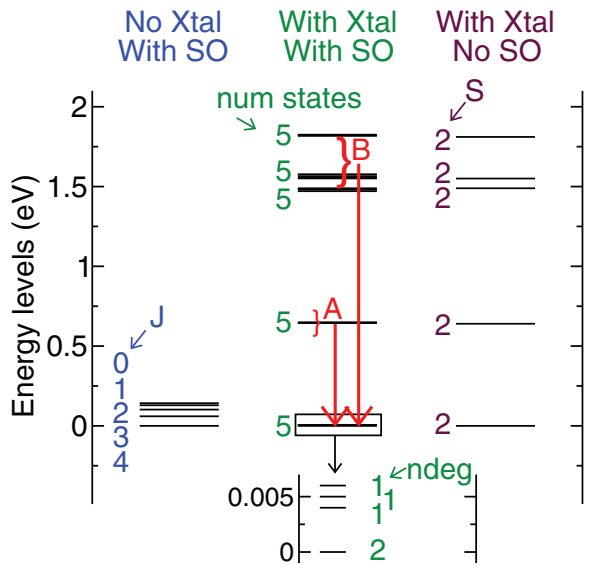

FIG. 7. (Color online) First 25 calculated multiplet levels of the initial state $2p^6 3d^6$. Column on the left: Coulomb and spin-orbit interactions only, with associated J number. Column in the middle: Coulomb, crystal field and spin-orbit interactions, with number of states close in energy that appear as one line. Inset: zoom into the lowest levels with crystal field interaction, and associated degeneracy ndeg. Column on the right: Coulomb and crystal field interactions only, with associated S number. A and B mark the two dominant dd excitation peaks seen in the experiment.

it also appears necessary to allocate a substantially shorter lifetime, corresponding to a larger linewidth, to the core-hole states after the L_3 pre-edge in order to simulate the relative resonance behavior of the set of peaks labeled A and B in Fig. 2. Like for XAS, the effective core-hole linewidth includes nonintrinsic effects; in this case, bandlike contributions play a substantial role. Unless otherwise stated, RIXS spectra in this paper have been calculated with a core-hole linewidth of 0.2 eV increased linearly to 0.4 eV also around 707.4 eV. The final-state Lorentzian linewidth was chosen to be 100 meV. No attempt was made to simulate instrumental broadening.

2. *Boltzmann weighting*

The temperature dependence of the spectra may have various causes. One effect related to temperature is the population of the first excited states of $2p^6 3d^6$ and their contribution to the dipolar transitions to the core-hole state. The XAS and RIXS spectra in this work are simulated at a temperature T by adding incoherently those contributions, weighted by the Boltzmann factor $\exp^{-\frac{\epsilon_i}{k_B T}}/Z$, where ϵ_i is the excitation energy of the ith state, k_B is the Boltzmann constant, and Z is the partition function.

3. *Average over orientations*

In order to compare the simulated spectra with the experiments, an averaging over the orientations within the b-c plane that accounts for the mosaicity has to be made. As no detailed information on the distribution of orientations could be obtained, the average was taken between the spectrum calculated with the scattering plane corresponding to a-b (geometrical set up 1), and that corresponding to a-c (geometrical set up 2). In the former case, the vertical incoming light polarization is along the rungs of the Fe ladders (c axis), in the latter case, along the legs of the Fe ladder (b axis). The resulting XAS and RIXS calculated spectra at 15 K are shown in Figs. 6(b) and 2(c), respectively, with the peak positions showing very good agreement with experiments. These figures are discussed in greater details in the following section.

V. MULTIPLET RESULTS

In this section, the calculated multiplet structure and resulting spectra are discussed. First, some features of the Fe L_3- and L_2-edge XAS are analyzed. The energy levels of the initial state are then examined in details. Next, the dd excitations of the Fe L_3-edge RIXS spectra are discussed with respect to the polarization directions. Finally, a mechanism leading to the peculiar temperature dependence of the dominant dd-excitation peaks is presented.

A. XAS spectra

The Fe L_3- and L_2-edge XAS spectrum in Fig. 6(b) exhibits a shoulder at 707.1 eV, a spectral feature that is prominent in the insulator Fe_2O_3 with Fe $3d^5$ valence configuration, but entirely washed out in metallic Fe and the Fe pnictides.[21] Figure 6(a) shows the effects of adding spin-orbit coupling (3, green curve) to the Coulomb interactions (2, red and 1, black curves) for Fe L_3- and L_2-edge XAS. As can be seen in the bottom lines (4, turquoise), the inclusion of the crystal field effects does modify the spectrum, but the presence of the shoulder peaks are caused primarily by the Coulomb and spin-orbit coupling. The curves in Fig. 6(a) have been individually rescaled for clarity and calculated at a constant, artificially small Lorentzian broadening.

B. Energy levels of initial state

The multiplet structure of the initial state $2p^6 3d^6$ is intricate, with the crystal field mixing orbitals in a nontrivial manner. The levels of the 25 lowest energy states are plotted in Fig. 7. The three columns of the figure show the levels with the crystal field and the spin-orbit interactions either switched on or off. The crystal field has been switched off for the column on the left-hand side. In that case, J is a good quantum number, and the Fe d^6 electrons exhibit a ninefold degenerate ground state with $J = 4$. The four subsequent excited states could be identified as having $J = 3,2,1,0$, in order of increasing energy. Switching the crystal field back on but setting spin-orbit coupling to zero produces the levels pictured on the right-hand side of Fig. 7, with S a good quantum number. The $S = 2$ ground state suggests the Hund's rule compliant ^5D as a ground state for the isolated atom, with the orbital moment however expected to be strongly affected by the crystal field. The approximately tetrahedral arrangement of the first-neighbor shell of the Fe atom may lead to the hasty conclusion that the two lowest levels on the right-hand side of the figure can be attributed to e_g orbitals and the three further levels to t_{2g} orbitals. The Fe atoms form a ladder structure, which together with the tetrahedral neighbors, leave no symmetry element at the Fe site, even if the distortions were

TABLE I. Expectation value M_J, M_S, and M_L of the operator J_Z, S_Z, and L_Z, respectively, along the crystallographic axis a, b, and c, for the twofold degenerate ground state.

Projection axis	M_J	M_S	M_L
a	−2.32, 2.32	−1.98, 1.98	−0.34, 0.34
b	−0.02, 0.02	−0.02, 0.02	−0.00, 0.00
c	−0.18, 0.18	−0.15, 0.15	−0.03, 0.03

neglected. It is, however, possible to attribute some character to the levels on the right-hand side of Fig. 7 by analyzing the energy levels for a single d electron in the crystal field. In the nonrelativistic limit, the differences in energy between the d^1 levels are identical to those of the lowest levels of the d^6, with naturally different multiplicities. Even in an orientation close to the standard orientation for a regular tetrahedron, all levels for the d^1 are mixtures of all the standard d orbitals d_{xy}, d_{yz}, d_{xz}, d_{z^2}, and $d_{x^2-y^2}$. Some components, however, strongly dominate each level with weights ranging from 94 to 99%. For d^1, the ground state on the right-hand side of Fig. 7 has mostly e_g character, and the next-level $t_{2g}(d_{yz})$ character. The next two levels are mixing e_g with $t_{2g}(d_{xy})$, while the last level has predominantly $t_{2g}(d_{xz})$ character.

With both the crystal field and the spin-orbit coupling applied, neither J nor S are conserved any longer, and no states can be characterized unambiguously. These levels are plotted in the middle column of Fig. 7, with the inset zooming into the lowest levels. The projection of the operator $\langle S_Z \rangle$ on the three crystallographic axis allows, however, the identification of a as the easy axis for the twofold degenerate ground state, with M_S highest along that axis. Table I collects the expectation values of J_Z, S_Z, and L_Z along a, b, and c. As plotted in the middle of Fig. 7, the crystal field has split the ground state into four states, separated only by a few meV, so that these states are populated at room temperature. The expectation value for the angular momentum operators are identically zero for the three singly degenerate excited levels. From this figure, it can be expected that a group of RIXS peaks (A) may appear at 0.65 eV energy loss and another (B) at around 1.5 eV, provided the dipole transitions *via* the core-hole states allow it. Since the levels in the middle of Fig. 7 are not pure states with respect to the quantum numbers but mixtures of them, weakly allowed transitions will be possible.

C. RIXS spectra

Similarly to the measurements of Fig. 2(a), the calculated RIXS spectra at 15 K across the Fe L_3 edge, Fig. 2(c), show at the pre-edge the dominance of the group of peaks A at 0.65 eV, followed at the post-edge by the enhancement of the group of peaks B at 1.5 eV. Both the measurements and the calculations in Fig. 2 are averages over the different contributions due to the suspected mosaicity of the sample, as well as over the outgoing light polarizations. Analyzing the different contributions separately reveals that the A peaks are dominant throughout the Fe L_3 sweep with the incoming light polarization along the crystallographic c axis (nearly parallel to the Fe ladder rungs) and the outgoing polarization in the a-b plane. On the other hand, the B peaks are dominant for incoming polarization in the a-b plane and outgoing polarization in the a-c plane. The full analysis taking the polarizations along crystallographic directions is summarized in Fig. 8. The B peaks are enhanced by the outgoing polarization along the a axis. The A peaks on the other hand are a spectral feature largely suppressed unless both polarizations are (or have components) in the b-c plane; this is understandable in view of the predominantly d_{yz} character of the final states A (see Fig. 7).

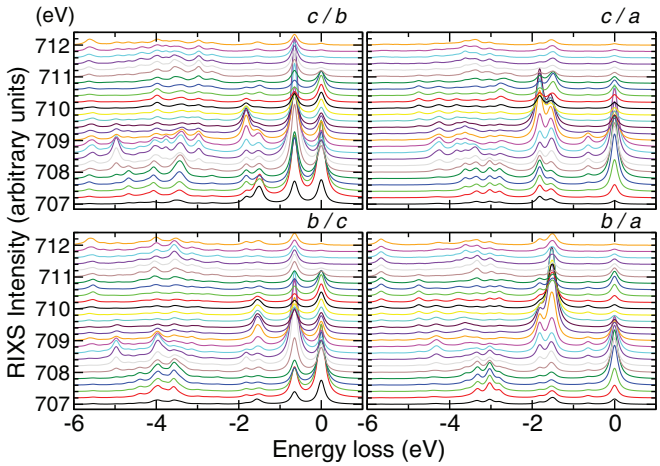

FIG. 8. (Color online) Calculated RIXS spectra at 15 K through the Fe L_3 edge. Incoming (respectively, outgoing polarization) along crystallographic axis, as indicated.

D. Temperature dependence

A close inspection of the temperature dependence of the measured RIXS spectra shows that the heights of the peaks do not vary in a simple manner with the temperature. Below 300 K, the peak B ($\hbar\omega_i = 708.8$) appears temperature independent, while the peak A ($\hbar\omega_i = 707.1$) decreases in height as the temperature increases, Fig. 4. In a simple case, it is expected that the Boltzmann factor lowers the height of a peak as the temperature goes above 0 K. As the temperature increases, the relative spectral weight for the allowed transition between the ground state and the excited state decreases, causing the decrease in the peak height.

If, however, both the states just above the ground state and the excited states are forming densely spaced multiplet levels, then there exists the possibility of creating new dipole-allowed transitions. Thermal population of the higher levels can lead to the appearance of spectral features at elevated temperature. The depopulation of the ground state and low levels can also lead to a reduction of certain features of the low-temperature spectrum. Those new allowed processes will cause the appearance of new peaks. This is likely to happen in $BaFe_2Se_3$, where several close levels have appeared because of the crystal field splitting, each level containing contributions from several orbitals. Once a new peak appears, its height will at first grow with increasing temperature, with weight transferred to it from the ground state. This effect is illustrated in Fig. 9(a1), for incoming photons at energy 709.1 eV. In Figs. 9(a1) and 9(a2), for clarity, the incoming polarization is along b and the outgoing polarization along c. The ground state is twofold degenerate, contributing the peaks plotted

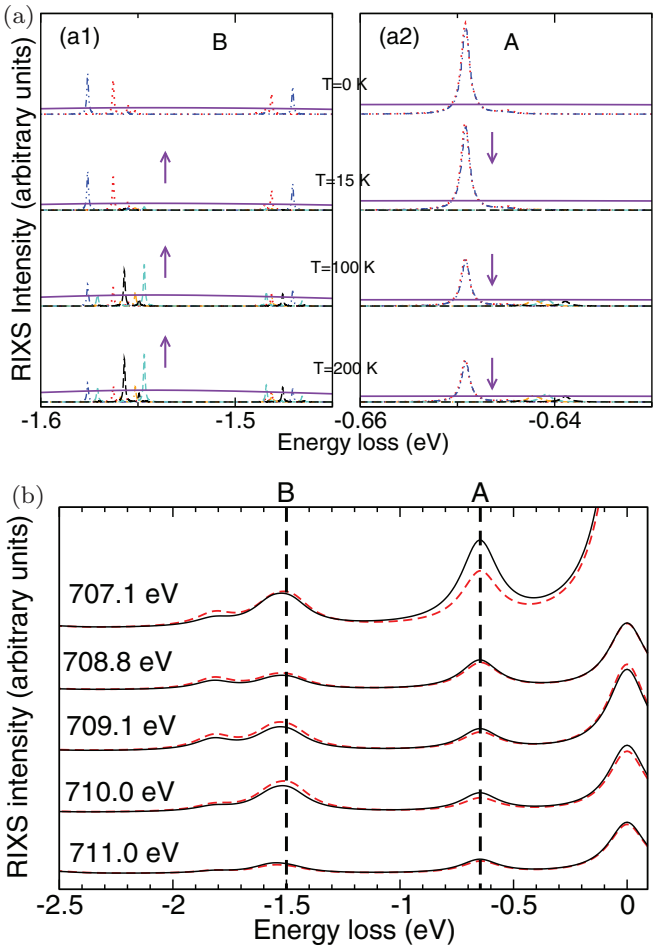

FIG. 9. (Color online) Calculated temperature dependence of the Fe L_3 RIXS spectrum using Boltzmann weighting. (a) Decomposition of peaks (solid violet line) into components (in order of increasing energy: red dots and blue dot-dot-dashes, orange dash-dash-dots, turquoise short dashes, and black long dashes) at different temperatures: (a1) B peaks at 709.1 eV incident energy and (a2) A peaks at 707.1 eV incident energy. Incoming polarization is along the b axis and outgoing polarization along the c axis. (b) 0 K (solid black), and 200 K (dashed red) at incident energies 707.1, 708.8, and 709.1 eV, for the average geometry.

respectively as dotted (red) and dot-dot-dashed (blue) lines in Fig. 9(a). At 0 K, these are the only possible contributions. At $T = 15$ K, all five levels shown in the inset of Fig. 7 are participating. Their contributions to the spectra in Fig. 9(a) are drawn as dash-dash-dotted (orange), short-dash (turquoise) and long-dash (black) lines, in order of increasing energy. At this temperature, new peaks have started to emerge, but most of the weight still rests with the original peaks. As the temperature increases further, the two original peaks lose weight in favor of the new ones. As the levels in this compounds are bunched up together below the experimental resolution threshold, both the A and B peaks appear as a sum of those components. The solid violet curves in Fig. 9(a) mark this summation, using a realistic final-state broadening of 100 meV. As can be seen in Fig. 9(a2), for 707.1 eV incoming photon energy at the A peaks, the loss of weight of the two original peaks is not compensated by the new peaks, whereas the opposite is true for 709.1 eV incoming photon energy at the B peaks, Fig. 9(a1).

These effects can be partially compensated when averaging over the polarization directions. However, an increase of the core-hole linewidth parameter from 0.2 to 0.7 eV after the L_3 pre-edge produces a better fit. It should be noted that a constant core-hole linewidth is normally expected for this range of photon energy, but that an increase from 0.2 to 0.4 eV reproduces the post L_3 edge resonance of the B peaks better (see Fig. 2). This effective, and peculiar dependence on core-hole lifetime suggests that both the post L_3 edge measured resonance and B peaks temperature behavior are strongly affected by the fluorescence and are not an intrinsic multiplet effect.

In Fig. 9(b), calculations comparing the 0 (solid black) and 200 K (dashed red) are plotted, averaging over the polarization directions which simulate the experimental conditions. In this case, like in the experimental results in Fig. 4, the peak A exhibit a small temperature dependence at photon energy 707.1 eV, while the peak B remains largely unaffected.

VI. CONCLUSION

In conclusion, we have performed RIXS measurements at the Fe L_3 edge of $BaFe_2Se_3$. A mixed character between a band material and a correlated material appears in our spectra, showing clear dd excitations typical of correlated iron oxides, in addition to a broad fluorescence line. The substantial broadening at 300 K is consistent with the system entering a nonmagnetic phase of increased metallicity, possibly undergoing an insulating to metal transition. Below 300 K, the temperature dependence of peaks measured near and after the Fe L_3 edge as the system enters into the AFM phase can be understood from the interplay of the various contributions of the low-lying initial states that are thermally occupied. This suggests that the temperature dependence of RIXS measurements could be more widely used for exploring the low-lying energy states of solid state compounds, even if their energy scale is directly inaccessible to the current RIXS instruments.

Crystal-field multiplet calculations successfully reproduce the positions of the sharp peaks. The fitting parameters such as charges and scaling parameters nonetheless point to a strong bonding environment. Moreover, the core-hole widths applied to the RIXS calculations are indicative of an interplay with the bands. Therefore weakly correlated band excitations and localized multiplet resonances coexist in $BaFe_2Se_3$.

ACKNOWLEDGMENTS

This work was performed at the ADRESS beamline of the Swiss Light Source at the Paul Scherrer Institut, Switzerland. This project was supported by the Swiss National Science Foundation (SNSF) and its National Centre of Competence in Research MaNEP. C.M. acknowledges also support by the SNSF under Grant No. PA00P2_142054, and A.U. the support of the SNF Grant No. 200021-129970.

*thorsten.schmitt@psi.ch

[1] Y. Kamihara, T. Watanabe, M. Hirano, and H. Hosono, J. Am. Chem. Soc. **130**, 3296 (2009).

[2] M. Rotter, M. Tegel, and D. Johrendt, Phys. Rev. Lett. **101**, 107006 (2008).

[3] F.-C. Hsu, J.-Y. Luo, K.-W. Yeh, T.-K. Chen, T.-W. Huang, P. Wu, Y.-C. Lee, Y.-L. Huang, Y.-Y. Chu, D.-C. Yan *et al.*, Proc. Natl. Acad. Sci. USA **105**, 14262 (2008).

[4] A. Damascelli, Z. Hussain, and Z.-X. Shen, Rev. Mod. Phys. **75**, 473 (2003).

[5] J. Orenstein and A. Millis, Science **288**, 468 (2000).

[6] M. Norman, D. Pines, and C. Kallin, Adv. Phys. **54**, 715 (2005).

[7] K.-J. Zhou, Y.-B. Huang, C. Monney, X. Dai, V. N. Strocov, N.-L. Wang, Z.-G. Chen, C. Zhang, P. Dai, L. Patthey, J. van den Brink, H. Ding, and T. Schmitt, Nat. Commun. **4**, 1470 (2013).

[8] C. Zhang, M. Wang, H. Luo, M. Wang, M. Liu, J. Zhao, D. L. Abernathy, T. A. Maier, K. Marty, M. D. Lumsden, S. Chi, S. Chang, J. A. Rodriguez-Rivera, J. W. Lynn, T. Xiang, J. Hu, and P. Dai, Sci. Rep. **1**, 115 (2011).

[9] D. J. Singh and M.-H. Du, Phys. Rev. Lett. **100**, 237003 (2008).

[10] E. Dagotto and T. Rice, Science **271**, 618 (1996).

[11] T. Vuletic, B. Korin-Hamzic, T. Ivek, S. Tomic, B. Gorshunov, M. Dressel, and J. Akimitsu, Phys. Rep. **428**, 169 (2006).

[12] A. Krzton-Maziopa, E. Pomjakushina, V. Pomjakushin, D. Sheptyakov, D. Chernyshov, V. Svitlyk, and K. Conder, J. Phys.: Condens. Matter **23**, 402201 (2011).

[13] J. M. Caron, J. R. Neilson, D. C. Miller, A. Llobet, and T. M. McQueen, Phys. Rev. B **84**, 180409(R) (2011).

[14] M. V. Medvedev, I. A. Nekrasov, and M. V. Sadovskii, JETP Lett. **95**, 33 (2012).

[15] H. Lei, H. Ryu, A. I. Frenkel, and C. Petrovic, Phys. Rev. B **84**, 214511 (2011).

[16] J. Schlappa, T. Schmitt, F. Vernay, V. Strocov, V. Ilakovac, B. Thielemann, H. Ronnow, S. Vanishri, A. Piazzalunga, X. Wang *et al.*, Phys. Rev. Lett. **103**, 047401 (2009).

[17] J. Schlappa, K. Wohlfeld, K. Zhou, M. Mourigal, M. Haverkort, V. Strocov, L. Hozoi, C. Monney, S. Nishimoto, A. Singh, S. Revcolevschi *et al.*, Nature (London) **10**, 974 (2012).

[18] A. Uldry, F. Vernay, and B. Delley, Phys. Rev. B **85**, 125133 (2012).

[19] V. N. Strocov, T. Schmitt, U. Flechsig, T. Schmidt, A. Imhof, Q. Chen, J. Raabe, R. Betemps, D. Zimoch, J. Krempasky *et al.*, J. Synchrotron Radiat. **17**, 631 (2010).

[20] G. Ghiringhelli, A. Piazzalunga, C. Dallera, G. Trezzi, L. Braicovich, T. Schmitt, V. N. Strocov, R. Betemps, L. Patthey, X. Wang *et al.*, Rev. Sci. Instrum. **77**, 113108 (2006).

[21] W. L. Yang, A. P. Sorini, C.-C. Chen, B. Moritz, W.-S. Lee, F. Vernay, P. Olalde-Velasco, J. D. Denlinger, B. Delley, J.-H. Chu *et al.*, Phys. Rev. B **80**, 014508 (2009).

[22] A. Kotani and S. Shin, Rev. Mod. Phys. **73**, 203 (2001).

[23] T. Schmitt, L.-C. Duda, M. Matsubara, M. Mattesini, M. Klemm, A. Augustsoon, J.-H. Guo, T. Uozumo, S. Horn, A. Ahuja *et al.*, Phys. Rev. B **69**, 125103 (2004).

[24] L. J. P. Ament, M. van Veenendaal, T. P. Devereux, J. P. Hill, and J. van den Brink, Rev. Mod. Phys. **83**, 705 (2011).

[25] Formally, they do not appear in the gap of $BaFe_2Se_3$ and thus should be rather named *dd* resonances.

[26] I. Jarrige, T. Nomura, K. Ishii, H. Gretarsson, Y.-J. Kim, J. Kim, M. Upton, D. Casa, T. Gog, M. Ishikado *et al.*, Phys. Rev. B **86**, 115104 (2012).

[27] C. Monney, K. Zhou, H. Cercellier, Z. Vydrova, M. Garnier, G. Monney, V. Strocov, H. Berger, H. Beck, T. Schmitt *et al.*, Phys. Rev. Lett. **109**, 047401 (2012).

[28] N. Ashcroft and N. Mermin, *Solid State Physics* (Thomson Learning, London, UK, 1976).

[29] B. Saparov, S. Calder, B. Sipos, H. Cao, S. Chi, D. J. Singh, A. D. Christianson, M. D. Lumsden, and A. S. Sefat, Phys. Rev. B **84**, 24 (2011).

[30] C. Monney, V. Bisogni, K. Zhou, R. Kraus, V. Strocov, G. Behr, J. Malek, R. Kuzian, S.-L. Drechsler, S. Johnston *et al.*, Phys. Rev. Lett. **110**, 087403 (2013).

[31] B. Delley, J. Chem. Phys. **92**, 508 (1990).

[32] B. Delley, J. Chem. Phys. **113**, 7756 (2000).

[33] J. P. P. Perdew, A. Ruzsinszky, G. I. Csonka, O. A. Vydrov, G. E. Scuseria, L. A. Constantin, X. Zhou, and K. Burke, Phys. Rev. Lett. **100**, 136406 (2008).

[34] H.A. Kramers and W. Heisenberg, Z. Phys. **31**, 681 (1925).

[35] D. M. Pease, Phys. Rev. B **44**, 6708 (1991).